Cloud-aerosol interactions for boundary layer stratocumulus in the Lagrangian Cloud Model

M. Andrejczuk,[1] W. W. Grabowski,[2] J. Reisner,[3] and A. Gadian[1]

Received 23 March 2010; revised 1 September 2010; accepted 7 September 2010; published 30 November 2010.

[1] Lagrangian Cloud Model (LCM) is a mixed Eulerian/Lagrangian approach to atmospheric large eddy simulation (LES), with two-way coupling between Eulerian dynamics and thermodynamics and Lagrangian microphysics. Since Lagrangian representation of microphysics does not suffer from numerical diffusion in the radius space and solves full droplet growth equations, it may be considered an alternative for the bin approach. This paper documents the development of LCM to include collision/coalescence processes. The proposed algorithm maps Lagrangian parcels collision/coalescence events on the specified two-dimensional grid, with the first dimension spanning aerosol radius and the second dimension spanning the cloud droplet radius. The proposed approach is capable of representation of aerosol activation, deactivation, transport inside the droplets, and processing by clouds and in the future may be used to investigate details of these processes. As an illustration, LCM with collision/coalescence is used to investigate effects of aerosols on cloud microphysics and dynamics for a marine stratocumulus cloud. Two extreme cases are considered that represent low and high aerosol concentrations. It is shown that the aerosol type significantly affects cloud microphysics as well as cloud dynamics. In agreement with previous studies, a larger entrainment rate is simulated for the high aerosol concentration. For the low aerosol concentration, intense collision/coalescence and drizzle modify the aerosol size distribution, reducing the concentration in the dry radius range of 0.02 to 0.2 μm and increasing the concentration for dry radii larger than 0.3 μm.

Citation: Andrejczuk, M., W. W. Grabowski, J. Reisner, and A. Gadian (2010), Cloud-aerosol interactions for boundary layer stratocumulus in the Lagrangian Cloud Model, *J. Geophys. Res.*, *115*, D22214, doi:10.1029/2010JD014248.

1. Introduction

[2] Anthropogenic aerosols are thought to introduce the indirect radiative forcing of -0.7 W m^{-2} (with a range of -1.8 to -0.3 W m^{-2}) with low level of scientific understanding [e.g., *Intergovernmental Panel on Climate Change*, 2007]. One of the ways to increase the understanding is to use numerical models to investigate cloud-aerosol interactions in as many physical settings as possible, focusing not only on the effects of aerosols on cloud microphysics and dynamics, but also on the processing of aerosols by clouds. For that, representation of cloud microphysics must be capable of handling aerosols properly, that is, including their impact on the cloud droplet spectrum as well as effects of cloud processing on the aerosol spectrum. Bin models that represent droplet spectrum in the space-and-radius Eulerian framework are typically used to investigate cloud-aerosol interactions [*Khairoutdinov and Kogan*, 1999; *Khain et al.*, 2004; *Ackerman et al.*, 2004; *Leroy et al.*, 2009]. Such models, however, feature significant challenges to realistically and efficiently represent droplet activation and deactivation as well as the curvature (Kelvin) and solute (Raoult) effects. They are often plagued by significant numerical artifacts, such as numerical spreading of the droplet/drop distributions, since only a relatively small number of bins is used (typically a few dozens).

[3] There are two major issues in bin models important for cloud-aerosol interactions: (1) representation of activation and deactivation of cloud droplets (which requires significant simplifications once growth by collision/coalescence takes place) and (2) droplet spectral broadening (which affects the width of cloud droplet spectra). Use of two-dimensional (2D) bin models spanning both droplet radius and aerosol radius space [e.g., *Clark*, 1973; *Chen and Lamb*, 1994; *Jacobson et al.*, 1994; *Bott*, 2000] eliminates in theory the source of the first error. However, 2D microphysics can only be used with a small number of bins in each dimension which in turn affects droplet spectral width. Realistic modeling of the spectral width is difficult because condensational growth leads to the narrowing of the droplet spectrum and applying a large number of bins may be the only solution.

[1]School of Earth and Environment, University of Leeds, Leeds, UK.
[2]Mesoscale and Microscale Meteorology Division, National Center for Atmospheric Research, Boulder, Colorado, USA.
[3]Earth and Environmental Sciences Division, Los Alamos National Laboratory, Los Alamos, New Mexico, USA.

0148-0227/10/2010JD014248

[4] Representation of drop evaporation leading to CCN deactivation and CCN removal by drops reaching the surface is essential in studies concerning aerosol processing by clouds, especially in long (several hours to many days) simulations. In current bin models, deactivated aerosol is placed in the previously activated aerosol bin starting from the smaller sizes as proposed by *Kogan et al.* [1995] or is assigned to the aerosol bin based on values obtained from fitting lognormal distribution to the deactivated aerosol volume [*Ackerman et al.*, 1995]. Such an approach is clearly inadequate once growth by collision/coalescence takes place since collision/coalescence increases not only mass of the droplet but also the mass of aerosol inside. Realistic representation of aerosol processing by precipitating clouds requires significantly more complex approaches (e.g., 2D bin grid as in work by *Jacobson et al.* [1994] or *Bott* [2000]). Numerical broadening of droplet spectra can affect aerosol processes as well because the broadening may lead to an early initiation of collision/coalescence and to a premature cloud dissipation (due to rain-out) or a change in the circulation regime.

[5] It is unclear what the sufficient number of bins has to be in order to eliminate numerical broadening. Limited study conducted in the past by *Khairoutdinov and Kogan* [1999] showed that microphysical schemes applying 29 and 57 bins gave similar results. However, since the authors did not show profiles of the spectral width, it is impossible to asses how the number of bins affected the width of the spectrum. The problem of spectral width modeling is complex and the number of bins required to accurately predict droplet growth by condensation may depend not only on the method used to calculate spectral change as demonstrated by *Khairoutdinov and Kogan* [1999], but also on the discretization of the bin space and the type of cloud under consideration (e.g., with more bins required for cumulus clouds, where updrafts are stronger and droplets grow to bigger sizes than in stratiform clouds). Modeling of cloud-environment interactions (i.e., entrainment and mixing) and their impact on droplet spectra poses even greater challenges [*Brenguier and Grabowski*, 1993; *Andrejczuk et al.*, 2004, 2006, 2009; *Hill et al.*, 2009].

[6] To avoid problems with numerical artifacts in the condensation model, *Andrejczuk et al.* [2008] proposed a novel Lagrangian approach in a traditional Eulerian Large Eddy Simulation (LES) model with the entire model (i.e., dynamics plus microphysics) referred to as the Lagrangian Cloud Model (LCM). A similar formulation, with microphysics formulated in Lagrangian framework was also developed recently by *Shima et al.* [2009] and was referred as the "super-droplet" method. In this approach, the gas phase is modeled using traditional continuous approach; aerosol/cloud droplets are tracked in the Lagrangian framework with a two-way interaction between Lagrangian parcels (each representing a large number of cloud droplets/aerosol particles) and the Eulerian gas phase. Using this approach, *Andrejczuk et al.* [2008] successfully simulated (in an idealized 2D setup) the relationship between the aerosol concentration and the cloud droplet number concentration from DYCOMS-II field campaign [*Twohy et al.*, 2005]. Since LCM applies particle-based Lagrangian approach, it correctly handles the activation/deactivation of cloud droplets and does not suffer from numerical diffusion in neither the radius space nor the physical space. It does suffer, however, from sampling errors due to representation of a large number of aerosol particles/cloud droplets by one Lagrangian parcel. This error affects mostly the standard deviation of total concentration with little effect on overall dynamics and microphysics [cf. *Andrejczuk et al.*, 2008, Figure 3]. It should be stressed that although the Lagrangian microphysics suffer less from numerical problems than the bin approach, the LCM is still affected by the numerical aspects because the gas phase (i.e., the LES model) applies the Eulerian approach. A fully Lagrangian model (i.e., for both dynamics and microphysics) would not be practical.

[7] This paper reports further LCM development to include collision/coalescence processes and LCM application to cloud-aerosol interactions in boundary layer stratocumulus clouds. Current model development efforts tend to represent aerosol processing by clouds in a simplified way, but detailed models of this process are needed. Since such models are often computationally intensive, they may serve as benchmarks for more simplified approaches. There are several examples of cloud-aerosol-dynamics interactions that are not fully understood, such as the relationship between evolving aerosol and cloud droplet concentration, formation and evolution of Pockets of Open Cells (POCs), effects of turbulent mixing on cloud dynamics and microphysics, or effects of giant and ultragiant aerosols on warm rain initiation. Studying these interactions requires microphysical models that represent not only effects of aerosols on cloud evolution, but also effects of clouds on aerosols. The model presented in this paper serves exactly that purpose.

[8] Section 2 presents details of the collision/coalescence treatment in the LCM and the setup of numerical simulations that illustrate application of the model to the stratocumulus cloud. Results are presented in section 3, followed by their brief discussion in section 4. A summary and possible future model developments in section 5 conclude the paper.

2. Numerical Model

[9] LCM for the case of the droplet activation and growth by diffusion of water vapor was discussed in considerable detail by *Andrejczuk et al.* [2008]. These aspects will not be repeated here. In section 2.1, we only discuss the way collision/coalescence is added to the existing LCM and follow with the details of the model setup in section 2.2.

2.1. Representation of Drop Collisions in LCM

[10] Throughout this paper we consider physical particles and Lagrangian parcels. The physical particle is a soluble aerosol particle, a cloud droplet (i.e., activated aerosol particle), or a drizzle drop. The Lagrangian parcel is meant to represent a collection of identical aerosol particles or cloud/drizzle drops. Each Lagrangian parcel has a set of properties, such as the position in the physical space, the number of physical particles it represents, their size and velocity. The Lagrangian parcel is assumed to move according to the predicted velocity of physical particles it represents. The properties of each Lagrangian parcel change due to the air motion and/or physical particle sedimentation, but also due to physical particle (aerosol/droplet/drop) growth or evaporation.

[11] When only condensation/evaporation is present as in work by *Andrejczuk et al.* [2008], Lagrangian microphysics

solves for a change of the radius r, 3 (2 in 2D) components of the parcel velocity $\mathbf{v}$, and the location $\mathbf{x}$ for each Lagrangian parcel. No information about parcel physical size is present in the model and parcel deformation by the flow is not taken into account. Location of the parcel determines to which computational grid box of the LES model the parcel belongs and corresponding forces are assigned to this grid box. Without collisions, the number of physical particles in each Lagrangian parcel does not change throughout the simulation. With collisions, the number of physical particles in the Lagrangian parcel does change, so the number needs to be predicted in addition to r, $\mathbf{v}$, and $\mathbf{x}$. More importantly, collisions produce new droplets and thus new Lagrangian parcels need to be introduced to represent properties of those newly created droplets or drops. The latter is a major concern as the number of Lagrangian parcels has to remain bounded for the problem to stay numerically tractable. A simple approach used here is to assume that a new Lagrangian parcel is created only if the number of drops it represents exceeds a specified threshold, as discussed later in this section.

[12] The procedure to include collision/coalescence into LCM involves three distinct steps. The first step selects Lagrangian parcels that are allowed to interact through collision/coalescence. In the second step, outcome of collisions between physical particles from Lagrangian parcels selected in the first step are mapped on the 2D (aerosol radius versus drop radius) microphysics grid. In the third step, a set of new Lagrangian parcels is created based on the results of the second step. These three steps are discussed in more detail below.

[13] In general, all droplets and drops from Lagrangian parcels present at a given point in space should be allowed to interact through collision/coalescence. In a numerical model, this implies that all Lagrangian parcels within a given grid box need to be included. This is how collision/coalescenece is represented in bin models, where uniform distribution of cloud droplets within a grid box is assumed. However, cloud droplets are not always distributed uniformly within the grid [*Andrejczuk et al.*, 2008, Figure 7]. Since information about parcel location is available in LCM, it can be used to take into account variability of the droplets distribution in space within the grid box. This is done by subdividing a grid box into smaller volumes, referred to as the "collisional grid boxes," and considering collisions within each collisional grid box separately. However, when dividing computational grid box into collisional grid boxes one needs to ensure that there is a sufficient number of Lagrangian parcels within each collisional grid box to create reasonable statistics of droplet collisions. Additionally, such a subdivision also leads to computational savings for a given number of Lagrangian parcels. If a computational grid box contains n Lagrangian parcels, then the number of collision calculations is $n(n-1)/2$. If each computational grid box is divided into eight collisional grid boxes (as is the case in simulations reported here) then each collisional grid box has $n/8$ Lagrangian parcels and the total number of collisions in the computational grid box (with eight collisional grid boxes) is then $n(n/8-1)/2$. This is approximately 8 times less compared to the case without the subdivision. Note that although information about the physical size of each Lagrangian parcel is not predicted, it is assumed that the parcel has volume equal to the volume of collisional grid, and can interact with all other parcels from the same collisional grid.

[14] Once Lagrangian parcels belonging to the same collision grid are identified in the first step, calculations of collision/coalescence between drops/droplets in all collisional grid boxes proceed using the 2D microphysics grid. Note that only parcels representing more cloud droplets then imposed threshold level n^T, discussed later, can collide. The 2D grid has $nca = 20$ bins for aerosols and $ncd = 30$ bins for cloud droplets, with corresponding ranges of 0.005–3 μm for the dry aerosol radius and 1–500 μm for the droplet radius. The droplet radius bins (in μm) are defined after *Morrison and Grabowski* [2007]:

$$r_m = 0.25 * (m-1) + 10^{(0.09*(m-1))}, \tag{1}$$

whereas the dry aerosol bins (in μm) are:

$$r_{0n} = 10^{(-2.3+0.15*(n-1))}. \tag{2}$$

The 2D microphysics grid is used in each model time step to store information about the outcome of droplet collisions and to generate new Lagrangian parcels.

[15] In the numerical representation of collision/coalescence, the algorithm considers two steps, with the first one dealing with existing parcels and second one responsible for new parcel creation. To explain how the numerical procedure works, let consider collisions between drops from two Lagrangian parcels i and j. The Lagrangian parcels represent drop numbers n_i and n_j, drop radii r_i and r_j, and dry aerosol radii r_{0i} and r_{0j}. The gravitational collision kernel for such drops is given by $K_{ij} = E_c\pi\,(r_i + r_j)^2|w_i - w_j|$ (where w_i and w_j are vertical velocities of drops i and j, and E_c is the collision efficiency). Collisions during the time interval Δt between drops from Lagrangian parcels i and j result in a creation of $N_{ij} = K_{ij}n_in_j\Delta t/V_c$ drops with the radius $(r_i^3 + r_j^3)^{1/3}$ and the dry aerosol radius of $(r_{0i}^3 + r_{0j}^3)^{1/3}$, where V_c is the volume of the collision grid. These radii determine the bin (m, n) on the 2D microphysical grid where the product of collisions is stored. The mass of the water and aerosol assigned to the bin (m, n) is given by $W_{mn} = \frac{4}{3}\pi\rho\,(r_i^3 + r_j^3 - r_{0i}^3 - r_{0j}^3)N_{ij}$ and $A_{mn} = \frac{4}{3}\pi\rho_s\,(r_{0i}^3 + r_{0j}^3)N_{ij}$, where ρ is the water density, and ρ_s is the aerosol density. This is repeated for collisions between all Lagrangian parcels within a given collisional grid box. As a result, a grid box (m, n) on the 2D microphysics grid contains outcomes of all possible collisions that lead to drops/aerosols in this very bin. This can be schematically written as

$$n_{mn} = \sum_{ij}^{(m,n)only} N_{ij}, \tag{3}$$

$$A_{mn} = \sum_{ij}^{(m,n)only} A_{ij}, \tag{4}$$

$$W_{mn} = \sum_{ij}^{(m,n)only} W_{ij}, \tag{5}$$

where the sum is calculated only over parcel indices i and j that contribute to the bin (m, n).

[16] For existing Lagrangian parcels (i.e., i or j above), the change of the number of cloud droplets the parcel k experiences is written as

$$\Delta n_k = -\frac{\Delta t}{V_c}\sum_{l=1}^{N} K_{kl} n_k n_l. \quad (6)$$

The drop and aerosol radii do not change. New parcels are created from the data on the 2D microphysics grid, with the number, drop radius, and aerosol radius derived from the cumulative number and mass of drops/aerosol in the bin. For instance, for the bin (m, n), the number of drops is given by n_{mn} and the corresponding aerosol radius and cloud drop radius are given by

$$r_{0mn} = \left(\frac{A_{mn}}{\frac{4}{3}\pi\rho_s n_{mn}}\right)^{1/3}, \quad (7)$$

$$r_{mn} = \left(\frac{W_{mn}}{\frac{4}{3}\pi\rho n_{mn}} + r_{0_{mn}}^3\right)^{1/3}. \quad (8)$$

It is important to point out that the procedure outlined above ensures that the change of the drop number in the system agrees with the initial number of drops modified by the number of drop collisions, and that the total mass of the aerosol and the total mass of the condensed water are exactly conserved.

[17] Because the algorithm assumes that a new Lagrangian parcel is created for each bin of the 2D microphysics grid, in theory $ncd \times nca$ new Lagrangian parcels can be created in each time step. In practice, however, the number is much smaller as typically only a few bins are filled. As a result of new parcel formation, the number of Lagrangian parcels increases despite the fact that the number of cloud droplets decreases due to collision/coalescence. Unless additional constraints are imposed in the above scheme, the increases of the total number of Lagrangian parcels will make the problem computationally intractable. Two types of constraints are considered. The first one is relatively simple; a new Lagrangian parcel is created for a given bin of the 2D microphysics grid only if the number of new droplets exceeds the imposed threshold, n^T. When the number of the new droplets is smaller than n^T, $n_{mn} = 0$ and corresponding numbers are not subtracted from existing parcels contributing droplets to this bin. The threshold n^T should be small to ensure that collisional growth is not impeded, but also as large as possible to ensure that the number of new Lagrangian parcels is kept at a manageable level. In current simulations, the threshold is taken as $n^T = 12.5$ that corresponds to about 1 cloud droplet per 100 m^3 for the smallest collision grid in the model.

[18] The second constraint is to limit the number of the parcels after the data from the 2D microphysics grid are mapped on the new Lagrangian parcels. This procedure considers the set of newly created parcels and merges them with already existing ones that have similar properties. Two Lagrangian parcels i and j are merged into a single one if: (1) they belong to the same size bin and the difference in droplet radii $|r_i - r_j|$ does not exceed the half width of the size bin; (2) they belong to the same aerosol bin and the difference in the dry aerosol radii $|r_{0i} - r_{0j}|$ does not exceed the half width of the corresponding aerosol bin; and (3) the sum of the particle number in the two Lagrangian parcels does not exceed 150% of the initial (assigned during model initialization) number of droplets each parcel typically represents. (The initial number is typically around $2 \times 10^{11}/3 \times 10^{10}$ for HIGH/LOW simulation; note that this number provides the context of the threshold value n^T introduced above). After merging two parcels, the new number of cloud droplets is the sum of both numbers, with the radii of cloud droplet and dry aerosol modified to conserve mass of water and aerosol, respectively. The physical properties (location, velocity) after merging are the same as the physical properties of one of the parcels.

[19] Comparison of model results using the collision algorithm described above with the continuous bin approach and with analytical solutions are presented in Appendix A.

2.2. Model Setup and Initial Aerosol Distribution

[20] Model setup closely follows that presented by *Andrejczuk et al.* [2008] and *Reisner and Jeffery* [2009]. The model is run in 3D, with $80 \times 80 \times 115$ grid points in x, y and z direction. Model grid length is 40 m in the horizontal directions and stretched in the vertical (the vertical grid length near the inversion is around 5 m). The model time step is 0.1s. Coriolis force is excluded and there is no source of aerosols. *Long* [1974] collision efficiencies are used.

[21] To speed up calculations, the model was first run for 1 h with bulk microphysics (see *Reisner and Jeffery* [2009] for the bulk microphysics description). Next, Lagrangian parcels were initiated over the entire domain from bulk model fields, by first evaporating all cloud water and then allowing condensation on aerosol particles within generated Lagrangian parcels. Subsequently, the model was run for 1 h without collisions to establish appropriate sizes of cloud droplets throughout the cloud. Finally, collision/coalescence was turned on and LCM was run for additional 7 h. The time in all analysis presented below is counted from the beginning of the simulation, including the bulk model run.

[22] Two simulations, referred as LOW and HIGH, are analyzed with corresponding total aerosol concentrations of 190 cm^{-3} and 1295 cm^{-3}. Aerosols with two-modal log-normal distributions are specified, with the mode radii of 0.011 and 0.06 μm, and the geometric standard deviations of 1.2 and 1.7. The aerosol concentrations for both modes are 125 cm^{-3} and 65 cm^{-3} for the LOW case (i.e., total of 190 cm^{-3}), the same as in work by *Ackerman et al.* [2009]. These are based on observations from flight RF01 of the DYCOMS-II field campaign. For HIGH, the concentration of aerosols in the accumulation mode is increased to 1170 cm^{-3} (i.e., 18 times the values in LOW) to get the total concentration of 1295 cm^{-3}. Both simulations apply the same initial conditions based on work by *Stevens et al.* [2005], with the aim to investigate model response to different aerosol distributions and cloud droplet number concentrations. Initially, 73×10^6 Lagrangian parcels are randomly distributed within the domain. This gives about 100 Lagrangian parcels per grid box. Because new Lagrangian

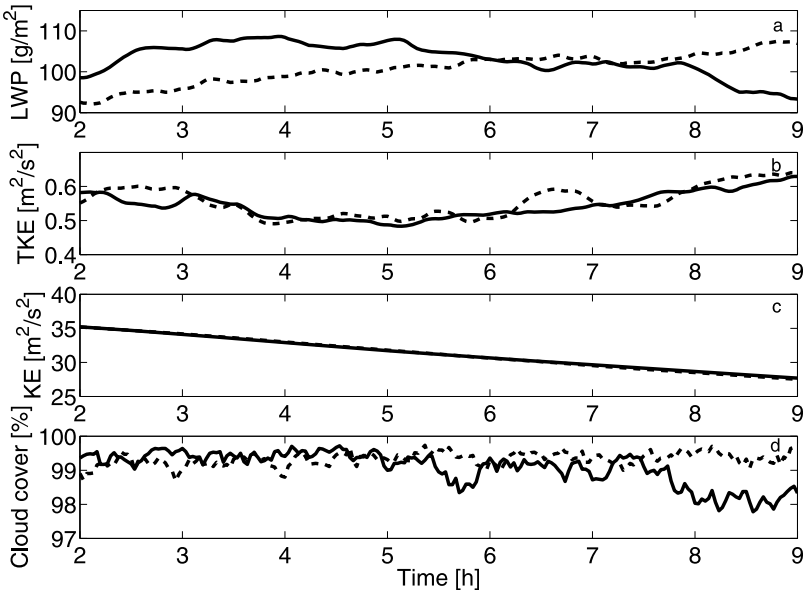

Figure 1. (a) Liquid water path (LWP), (b) turbulent kinetic energy (TKE), (c) mean kinetic energy (KE), and (d) cloud cover as a function of time for runs LOW (solid line) and HIGH (dashed line).

parcels are created during simulation, the number of parcels at the end of simulations is about 150×10^6 for both cases.

3. Results

3.1. Macroscopic Fields

[23] Figure 1 shows evolutions of selected macroscopic measures of the simulated stratocumulus-topped boundary layer for the LOW and HIGH simulations. The liquid water path (LWP) averaged over the whole domain shows different evolutions for LOW and HIGH simulations, see Figure 1a. For HIGH, the LWP increases gently during the whole simulation. For LOW, the LWP initially increases and then decreases after 4 h of the simulation. Neither the turbulent kinetic energy, $TKE = \frac{1}{2}\langle (u - \langle u \rangle)^2 + (v - \langle v \rangle)^2 + (w - \langle w \rangle)^2 \rangle$ (where $\langle \, . \, \rangle$ depicts the domain average), nor the mean kinetic energy, $KE = \frac{1}{2}(\langle u \rangle^2 + \langle v \rangle^2 + \langle w \rangle^2)$, show significant differences between LOW and HIGH. Cloud cover (defined as the percentage of model columns with LWP greater than 20 g m^{-2}) is initially similar for both simulations. With time it decreases from over 99% to about 98% in the second half of the LOW simulation. For the HIGH simulation, the cloud cover stays above 99% for most of the time.

[24] Spatial distributions of LWP at various times are shown in Figure 2. Figures 2a, 2b, and 2c show LWP for LOW at 3 h of the simulation (i.e., 1 h after collision/coalescence was turned on), at 4 h (when LWP for LOW is close to the maximum) and at 9 h, respectively. Figures 2d, 2e, and 2f show corresponding results for HIGH. At all times, LWP shows irregular structures and limited organization for both cases. Histogram (not shown) of the LWP shows that the decrease of the mean LWP at the end of the simulation in LOW is due to the increase of cloud-free/low LWP areas and decrease of the area with LWP above 90 g m^{-2}. For HIGH, there is no significant change in the LWP pattern and area with high LWP is increasing at the expense of low LWP areas.

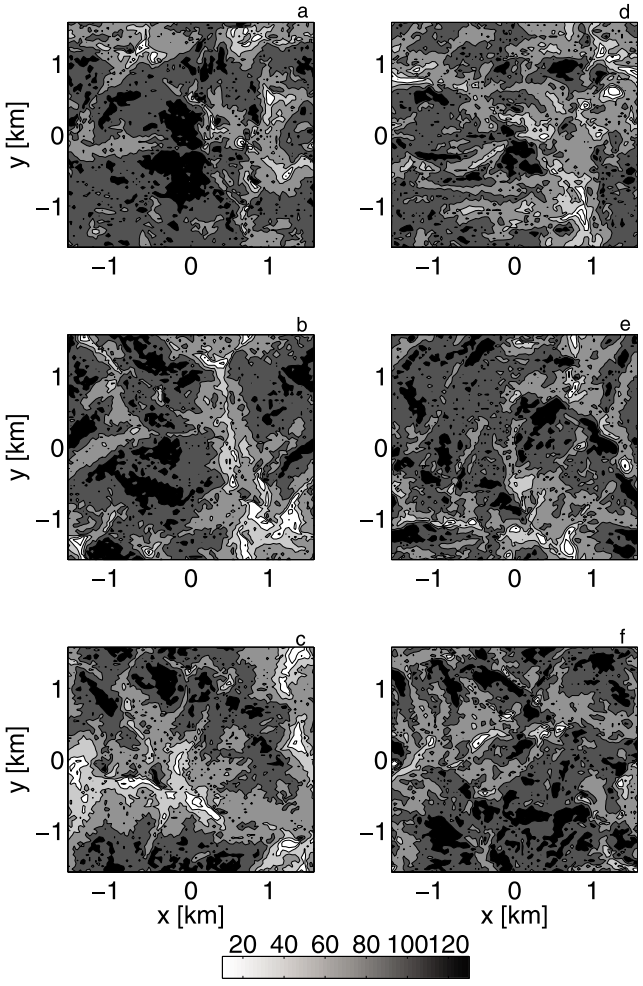

Figure 2. The LWP horizontal distribution after (a, d) 3 h, (b, e) 4 h, and (c, f) 9 h for LOW (Figures 2a–2c) and HIGH (Figures 2d–2f).

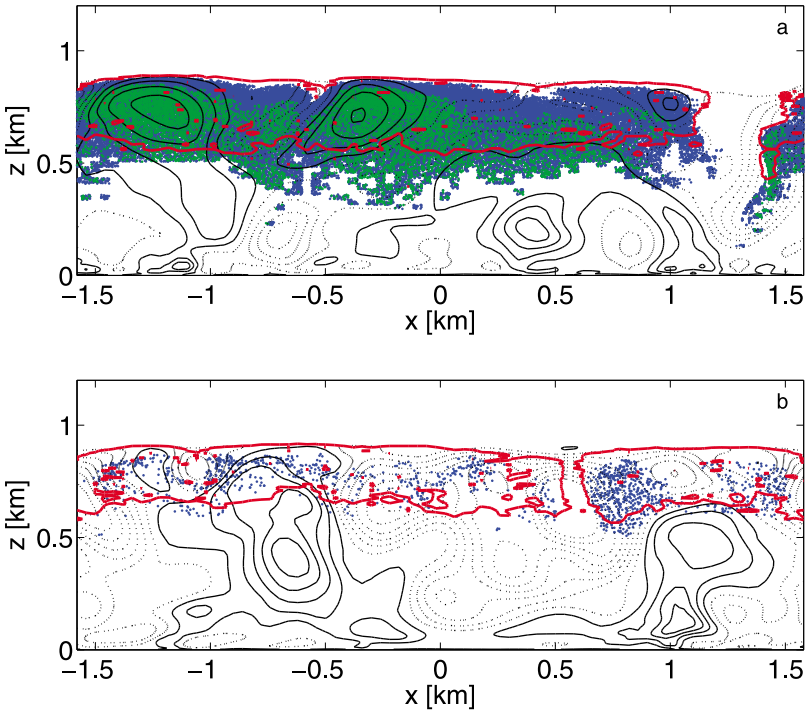

Figure 3. Vertical cross sections through model domain after 9 h of simulations: cross sections at (a) $y = -1180$ m for LOW and (b) $y = 420$ m for HIGH. Solid lines indicate positive velocities starting from 0.1 m/s with contour interval 0.2 m/s; dotted lines represent negative velocity starting from −0.1 m/s with the interval −0.2 m/s. The red line presents condensed water contour of 0.1 g/kg. Blue/green dots represent the locations of droplets bigger than 50/90 μm.

[25] Figures 3a and 3b show vertical slices (x–z) through the domain after 9 h for LOW and HIGH simulations. The slices are for y = −1.180 km and y = 0.420 km for LOW and HIGH, respectively, chosen to intersect cloud-free regions identified in Figure 2 at 9 h. Red contour shows cloud water mixing ratio of 0.1 g/kg (i.e., the cloud boundary), black solid (dashed) lines show positive (negative) vertical velocity with contour interval of 0.2 m s^{-1} (starting at either 0.1 or −0.1 m s^{-1}). Blue/green dots show locations of Lagrangian parcels featuring cloud drops with radius larger than 50/90 μm. Since such drops are created through collision/coalescence, each dot represents different number of drizzle drops. For the LOW simulation, Figure 3 shows signs of decoupling as two separate circulations seem to exist below and above the height of 500 m. For the HIGH simulation, updrafts and downdrafts connect the near-surface regions with the cloud aloft. The cloud structure is different in both runs, with relatively uniform cloud thickness for HIGH and thicker cloud in the region where drizzle is present for LOW. Cloud top is higher for HIGH and reaches almost 900 m. For both cases, areas with negative vertical velocity within the cloud show cloud clearing and cloud top lowering as a result of droplet evaporation in downdrafts. Limited drizzle is present for the high aerosol concentration, and most of it evaporates before reaching the ground.

[26] Profiles of the potential temperature (θ; Figure 4a) and water vapor mixing ratio (q_v; Figure 4b) after 9 h show different responses of the boundary layer to initial aerosol concentration. Since the difference in θ and q_v after 2 h is very small between LOW and HIGH, only temperature for LOW after 2 h is plotted with the gray solid line. For the low aerosol concentration, θ below the cloud at the end of the simulation is lower than after 2 h. This temperature reduction (about 0.5 K near the surface) is associated with drizzle evaporation below the cloud. For high aerosol

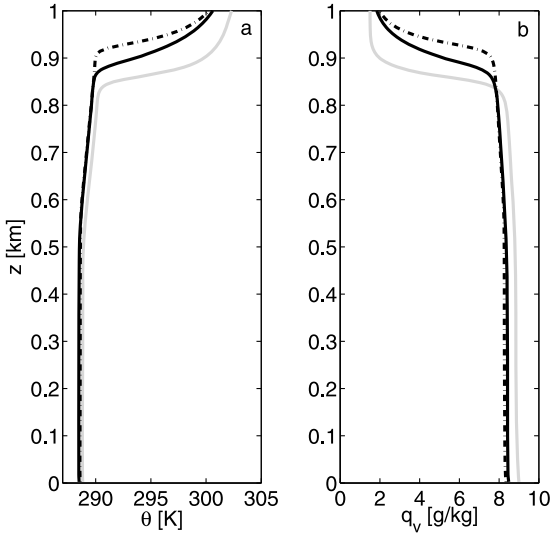

Figure 4. Profiles of (a) the potential temperature and (b) water vapor mixing ratio after 9 h for LOW (solid line) and HIGH (dash-dotted line). Light solid line shows profile for LOW after 2 h.

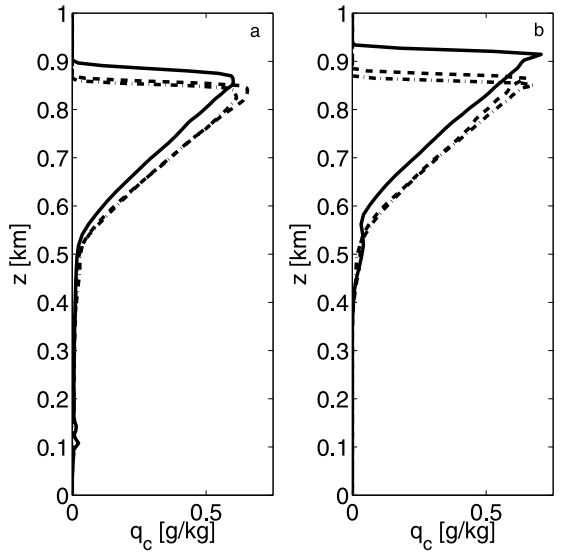

Figure 5. Profiles of the cloud water mixing ratio conditionally sampled over the region with $q_c > 0.001$ g/kg after 3 h (dash-dotted line), 4 h (dashed line), and 9 h (solid line) for (a) LOW and (b) HIGH.

concentration simulation HIGH, the temperature reduction is smaller (less then 0.2 K). The temperature inside cloud is approximately the same for both cases. For HIGH, the inversion is elevated compared to 2 h profile by about 50 m, with a smaller increase of the inversion height for LOW. Water vapor mixing ratio profiles (Figure 4b) show a reduction below the cloud for both solutions compared to the profile after 2 h. For HIGH, the reduction is more pronounced (about 0.5 g kg^{-1}) which is a sign of the layer drying due to the entrainment of drier air from above the inversion. For LOW, the reduction of boundary layer q_v is smaller, most likely because of the smaller entrainment rate in this case (defined after *Stevens et al.* [2003] as the change of the inversion height in both cases) and drizzle evaporation. Weaker gradient near the top of the boundary layer for LOW is associated with bigger variability of the cloud top height for this case.

[27] Profiles of the condensed water mixing ratio q_c after 2, 4, and 9 h are shown in Figure 5. The condensed water was conditionally sampled and only points with $q_c > 10^{-3}$ g kg^{-1} are included. Conditional sampling affects mostly the LOW case since more cloud-free areas are present in this case. Figure 5 shows that the maximum of q_c is higher for HIGH run. Significantly more drizzle is present beneath the cloud in the LOW case (the mixing ratio near the surface is around 0.006 g kg^{-1}). The drizzle is also present in the HIGH case but it is not captured by the conditional sampling because of the specified threshold. Another important feature in Figure 5 is the increase of the cloud top height, with the cloud top rising almost twice as fast between 4 and 9 h in the HIGH simulation when compared to LOW.

[28] Profiles of the variance w'^2 and the third moment w'^3 of the vertical velocity (where $w'(z) = w(z) - \overline{w}(z)$, where $\overline{w}(z)$ is the mean vertical velocity at the height z) for LOW (Figures 6a and 6c) and HIGH (Figures 6b and 6d) are presented. All profiles from hours 2 to 9, saved every minute, are plotted with light gray lines to show the variability; profiles after 2, 4, and 9 h are plotted with thick black dash-dotted, dashed, and solid lines, respectively. Figure 6 illustrates a significant variability of w'^2 and w'^3 at all levels within the boundary layer for both runs. For LOW, the range of instantaneous profiles of w'^2 seems larger than for HIGH, and profiles of w'^2 and w'^3 show a double-peak structure, with one peak below the cloud and additional peak within the cloud layer. Such a structure is typically a sign of the boundary layer decoupling [e.g., *Turton and Nicholls*, 1987]. For HIGH, the profiles show extrema of w'^2 and w'^3 within the cloud layer only.

3.2. Microphysics

[29] As a result of collision/coalescence, the mean cloud drop concentration tend to decrease in time. This is not only because coalescence of two droplets results in a single one, leading to formation of a large or giant CCN if the drizzle drop evaporates within the boundary layer, but also because development of drizzle leads to removal of CCN if a drizzle drop reaches the surface. It follows that the decrease of the mean droplet concentration depends on the initial aerosol concentration and thus on the initial droplet concentration. This is illustrated in Figure 7a which shows the evolution of the cloud droplet concentration normalized by the initial number of aerosol in the accumulation mode for the two cases considered in this paper. For the low aerosol concentration, the reduction of the droplet concentration is significant as the number of cloud droplets normalized by the initial number of aerosol in the accumulation mode drops from 80% to close to 30% during the 7 h. For the high aerosol concentration, there is almost no change in the mean cloud droplet concentration in time. Figure 7b shows evolution of the mass of aerosol normalized by the aerosol mass

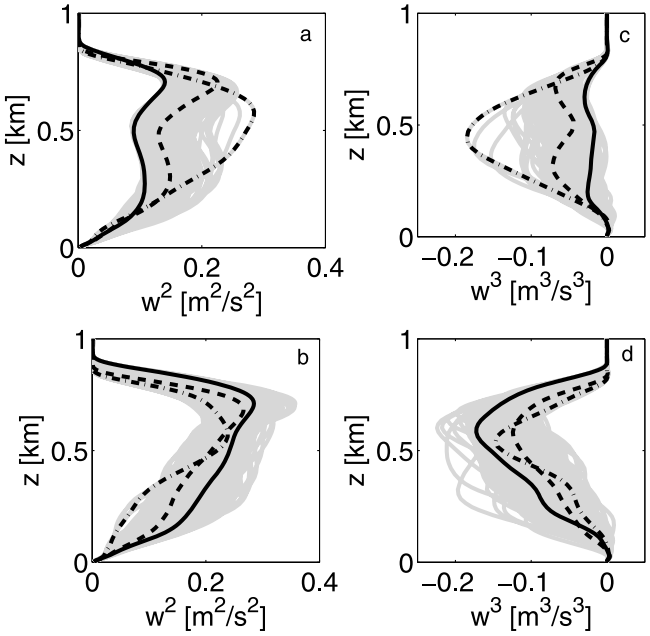

Figure 6. Profiles of w'^2 in (a) LOW and (b) HIGH, and profiles of w'^3 in (c) LOW and (d) HIGH. Gray lines shows all profiles from 2 to 9 h saved every 1 min. Dash-dotted, dashed, and solid lines are for profiles 2, 4, and 9 h, respectively.

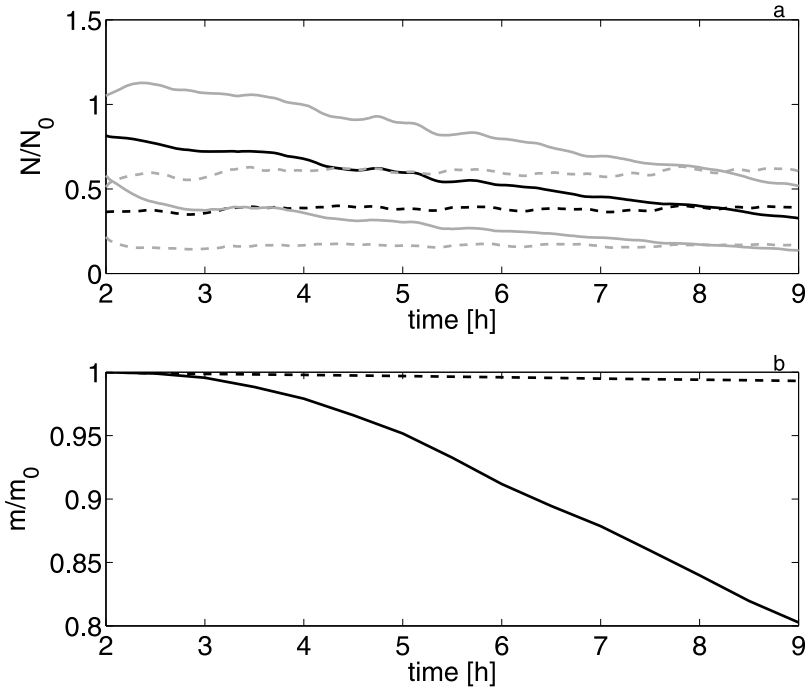

Figure 7. (a) Evolution of the mean cloud drop concentration normalized by the initial aerosol concentration in accumulation mode for LOW (solid line) and HIGH (dash-dotted line), with corresponding gray lines showing standard deviations starting from 2 h. (b) Evolution of the mass of the aerosol in the whole domain normalized by the mass at 2 h.

at 2 h. Similar to the mean cloud droplet concentration, there is little change in the mass for HIGH run. For LOW, on the other hand, the aerosol mass drops by 20% as a result of the removal of aerosol by drizzle reaching the ground. It has to be pointed out, however, that the simulations exclude aerosol formation within the boundary layer as well as aerosol fluxes from either the surface (model bottom) or the free atmosphere (model top). It is uncertain how neglecting aerosol sources impacts the reductions presented in Figure 7.

[30] Vertical profiles of the drop concentration, mean drop radius and standard deviation of the drop distribution for times of 3 and 9 h are shown in Figures 8 and 9 for LOW and HIGH simulations, respectively. Only points with total water mixing ratio larger than 10^{-3} g kg^{-1} are included in the analysis. For the LOW simulation (Figure 8), the drop concentration falls to less than 20 cm^{-3} at the end of the simulation, in agreement with results shown in Figure 7a. As anticipated, the reduction of the drop concentration leads to the increase of the drop mean radius within the cloud. The increase of the mean radius is also accompanied by the increase of the standard deviation (i.e., the spectral width) of the drop spectrum. Significantly larger mean drop sizes and spectral widths below the cloud are due to drizzle as the mean radius is larger than 30 μm and the standard deviation is larger than 10 μm.

[31] For the HIGH simulation (Figure 9), only small changes of the profiles are observed, with much higher drop concentrations (several hundred cm^{-3}), smaller drop size (reaching only 6.5 μm near the cloud top), and spectral width of just 1 to 2 μm. Note that the HIGH simulation does feature some drizzle, but it is only evident near the cloud base where the local water mixing ratio exceeds the threshold assumed in the conditional sampling. Another aspect worth pointing out in both simulations are entrainment zones near the cloud top, marked by increased standard deviations that result from droplet evaporation in warm and dry air entrained from above the cloud.

[32] The most important advantage of the approach presented in this paper is its ability to represent aerosol processing through collision/coalescence and aerosol deactivation.

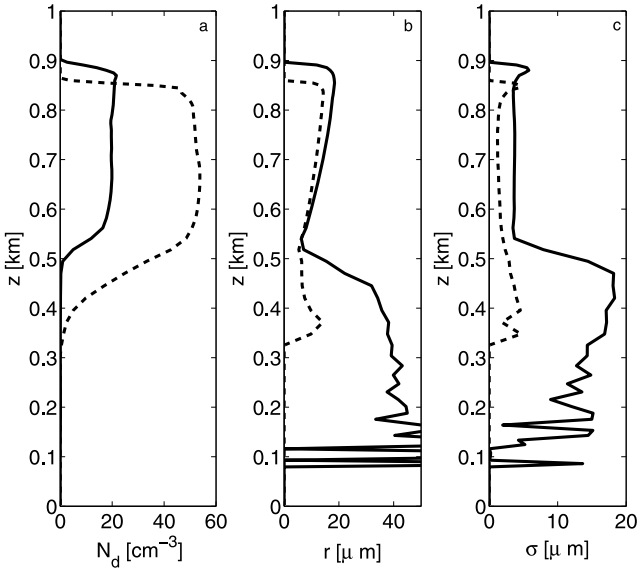

Figure 8. Vertical profiles of the cloud drop (a) concentration, (b) mean radius, and (c) standard deviation for LOW after 3 h (dash-dotted line) and 9 h (solid line).

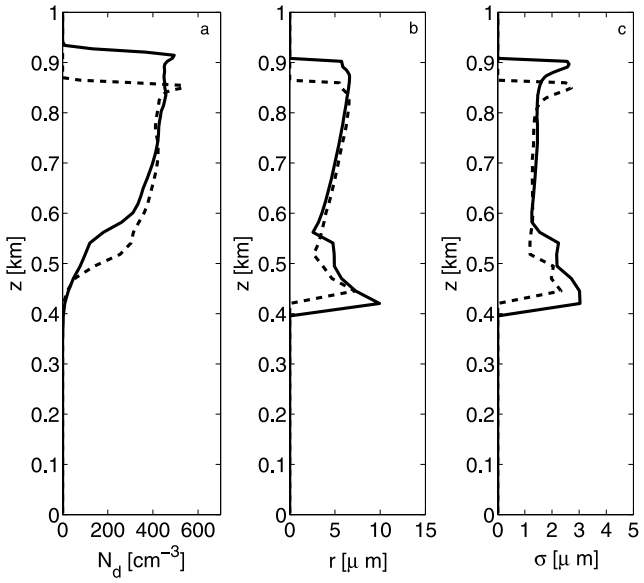

Figure 9. Same as Figure 8 but for the HIGH simulation.

Figures 10a and 10b show aerosol size distributions averaged over the entire domain after 3 (dashed line) and 9 (solid line) h of the simulations. Figures 10a and 10b illustrate an increase of aerosol concentration for radius above 0.3 μm (large and giant CCN) for the LOW simulation. At the same time, a reduction of aerosol concentration in the radius range of 0.02 to 0.2 μm is apparent. This implies that aerosols larger than 0.02 μm are activated and grow to sizes which enable collision/coalescence. Since in HIGH the cloud drop concentration is significantly higher and the mean drop radius is significantly smaller, collision/coalescence does not process aerosols as efficiently as in LOW. As a results, only small changes (within the thickness of the line in Figure 10b) of the aerosol distribution are observed for the largest aerosols only.

[33] With the cloud droplet concentration decreasing with time for the LOW simulation (see Figure 7a), the collision/coalescence becomes increasingly efficient and produces droplets with radius as large as 200 μm after 9 h. The shift of the spectral maximum toward larger radii is evident in the drop spectra (see Figure 10c). In contrast, insignificant changes in the drop distributions occur during the same time in the HIGH simulation, see Figure 10d.

4. Discussion

[34] Results from the 3D Lagrangian Cloud Model agree qualitatively with other models with size-resolving microphysics. For instance, *Stevens et al.* [1998] showed similar effects of intense drizzle on the stratocumulus cloud and boundary layer, with moistening and cooling of the subcloud layer. Heavy drizzle in LOW leads to the reduction of the cloud water inside the cloud toward the end of the simulation because of an efficient removal of the condensed water by drizzle. Arguably, the efficiency of aerosol processing by a drizzling cloud in the LOW simulation increases with time as reduced droplet concentration leads to increasingly efficient drizzle formation and consequently even more efficient aerosol processing. One can refer to this process as the aerosol-drizzle feedback. The amount of drizzle in the HIGH simulations was insufficient for the feedback to lead to appreciable effects during the simulation time.

[35] Model results demonstrate a strong impact of the initial aerosol concentration on cloud thickness and LWP. In general, the cloud is initially thicker and LWP is larger for low aerosol and cloud droplet concentrations. This holds true when collision/coalescence is present until drizzle becomes so heavy that it efficiently removes the condensed water from the cloud, as in the second half of the LOW simulation. The relation between the low cloud droplet concentration, high precipitation at the surface, and low LWP was already observed in numerical model by *Ackerman et al.* [2004] for DYCOMS-II. Time evolution of LWP may explain the inconsistency observed by

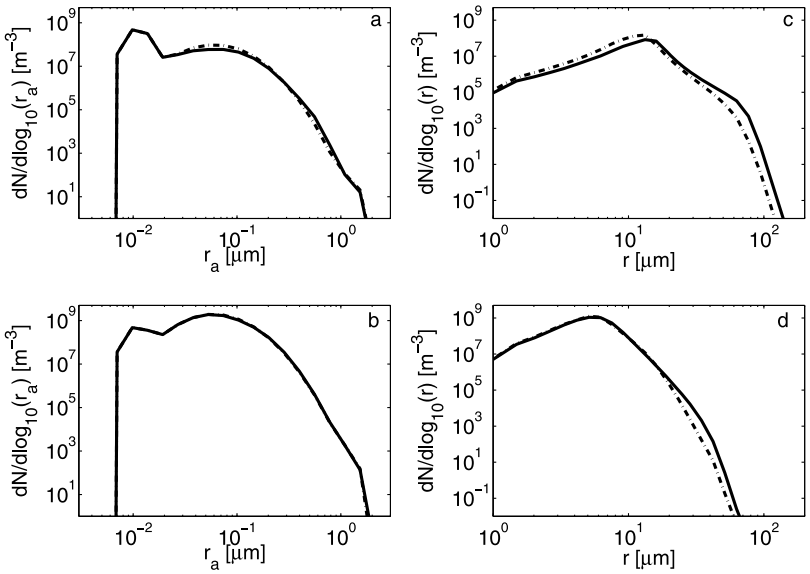

Figure 10. Aerosol spectra after 3 h (dash-dotted lines) and 9 h (solid lines) for (a) LOW and (b) HIGH, and cloud droplet spectra at the same times for (c) LOW and (d) HIGH.

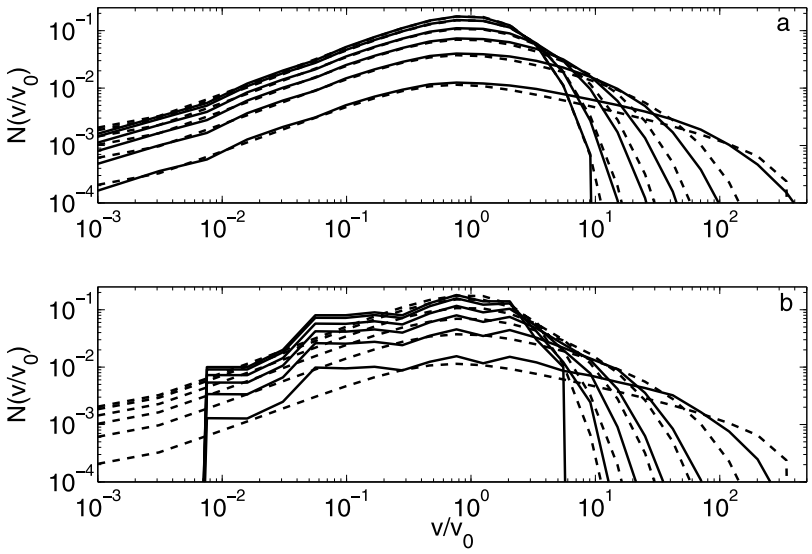

Figure 11. Initial distribution and solutions for times 69, 233, 450, 790, and 1500 s for the Golovin kernel (dashed line) and LCM scheme (solid line). (a) Solution with 100 parcels initially averaged over 100 realizations and (b) solution for 100 parcels initially.

Ackerman et al. [2004], where LWP initially increased with increasing cloud droplet concentration, and later, for cloud droplet concentrations larger than 30 cm^{-3}, started decreasing [cf. *Ackerman et al.*, 2004, Figure 1]. Changes in the cloud and flow may be large for low cloud droplet concentrations and averages taken for the latter case depend on time. For instance, LWP between hours 3 and 4 is larger for LOW run than for HIGH run, but situation is opposite for hours 8 and 9. The maximum of LWP for HIGH case is reached later than for LOW case, since more time is required to process aerosol and reach the stage when removal of water by the drizzle reduces LWP. The increase of LWP with decreasing aerosol concentration is anticipated before the onset of rapid removal of water by drizzle: the key is the sedimentation of cloud droplets which moves condensed water away from the very cloud top. *Bretherton et al.* [2007] suggest that droplet sedimentation decreases the cloud-top entrainment rate and thickens the cloud, and attributes it to the reduction of the "entrainment efficiency" with increasing mean droplet size. Results presented in this paper seem consistent with the discussions of *Stevens et al.* [1998], *Bretherton et al.* [2007] and *Ackerman et al.* [2004].

[36] The key feature of the approach presented here is that it is capable of representation of aerosol activation, deactivation, transport inside the droplets and processing by clouds; and in the future may be used to investigate details of these processes. Since aerosol processing leads not only to decrease of the aerosol concentration but also to the change of the aerosol distribution as illustrated by Figure 10, development of accurate parameterizations of this process for models applying simpler approaches (e.g., a double-moment warm rain scheme) may be difficult for low aerosol concentrations.

5. Summary and Outlook

[37] This paper extends the Lagrangian approach to model condensation in a LES model [*Andrejczuk et al.*, 2008] to the case of collision/coalescence. Incorporation of droplet collisions into the Lagrangian Cloud Model (LCM) requires additional considerations as new Lagrangian parcels need to be created at every model time step. The approach presented in this paper applies a 2D microphysics grid (aerosol radius versus drop radius) onto which the outcome of drop collisions from different Lagrangian parcels are mapped. Subsequently, new Lagrangian parcels are created based on the data from the 2D microphysics grid. The number of new Lagrangian parcels, the main concern when droplet collisions are considered, is limited to a manageable number by creating new parcels only when they represent more droplets than a specified threshold level and by merging parcels having similar properties.

[38] The resulting LCM has several advantages over traditional bin approaches. First, it is virtually free from numerical artifacts that often plague finite-difference spectral-density bin schemes. However, LCM does suffer from sampling errors when the number of Lagrangian parcels is small. Second, the extension to collisional growth of cloud and drizzle droplets allows for accurate representation of aerosol processing and removal. This aspect is highlighted in LCM simulations where model results for low and high aerosol concentrations are contrasted. When applied to simulations with significantly higher spatial resolution, LCM is capable of representing drop response to the flow accelerations and simulate, for instance, concentration inhomogeneities due to drop inertia. At the cloud microscale, such effects attracted considerable attention due to the impact of small-scale turbulence on collision/coalescence of cloud droplets [e.g., *Wang and Grabowski*, 2009, and references therein]. The impact of larger-scale turbulent eddies (say, tens of meters) on the motion and collisions of drizzle-size drops remains unclear and can be studied using the approach developed in this paper. The key point is that the Lagrangian parcel scheme solves for the drop velocity, in contrast to traditional

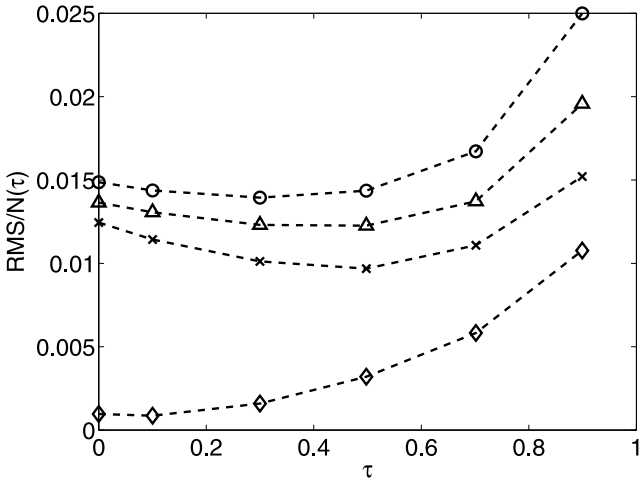

Figure 12. The RMS error normalized by number of cloud droplets as a function of nondimensional time for runs with 50 (crosses), 100 (circles), and 200 (triangles) parcels initially and run with 100 parcels averaged over 100 realizations (diamonds).

approaches which assume that the drop velocity is a vector sum of the air velocity and the terminal drop velocity.

[39] The treatment of droplet collisions as presented in this paper is fully conservative. It conserves the total water mass and total aerosol mass, and predicts the changes of the drop concentration as dictated by the number of droplet collisions. However, the LCM presented here is limited to warm rain processes only and to a single aerosol type. The algorithm can be extended to treat mixed phase clouds and to handle more than one aerosol type. This will require an expansion of the list of Lagrangian parcel properties and to increase the number of dimensions in the microphysics space (beyond the 2D used here) onto which effects of physical particle collisions are mapped. We plan to report on such developments in future publications.

Appendix A: Tests of the LCM Collision/ Coalescence Scheme

[40] Analytic solutions for the Golovin coalescence kernel [*Golovin*, 1963; *Scott*, 1963] are often used to validate numerical models. Figure 11 shows the time evolution of the cloud droplet distribution for the Golovin kernel using the LCM scheme and compares it to the analytic solution for times 69, 233, 450, 790 and 1500 s. In the numerical model, the volume of the air equal to 10^6 m^3 was assumed. A grid defined by equation (1) with 30 bins was used and models were run with time step of 0.5 s. In the numerical model a random number generator was used to generate initial droplet radii having an exponential distribution. Figure 11a shows the solution with 100 parcels used to represent the exponential distribution averaged over 100 realizations

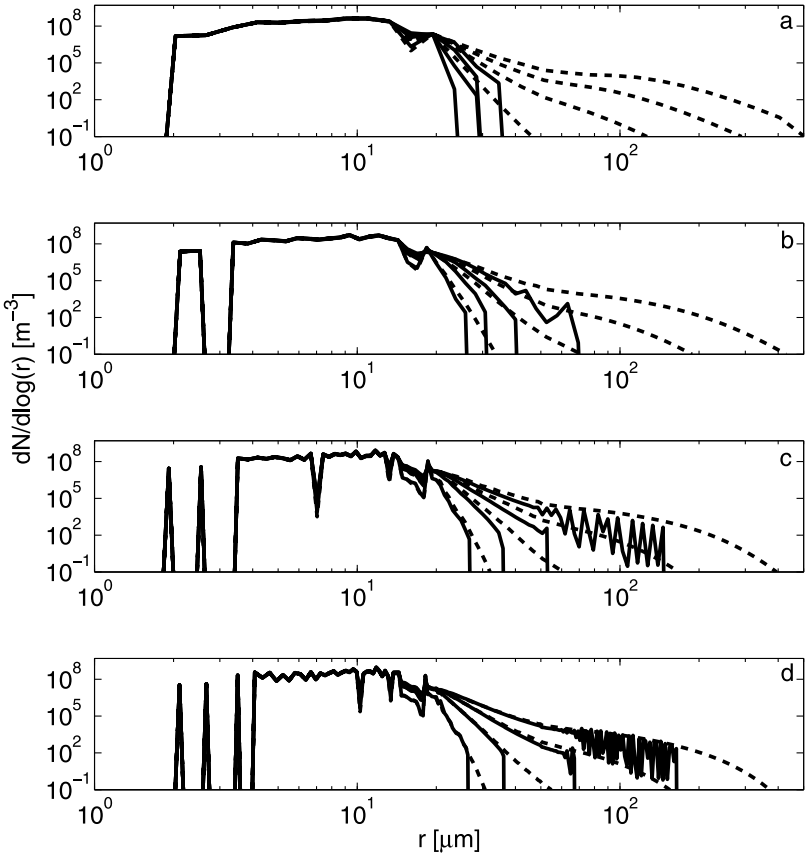

Figure 13. Solutions after 200, 800, 1400, and 2000 s for hydrodynamic kernel with Long collision efficiency for Bott scheme (dashed line) and LCM scheme (solid line) for (a) 30 bins, (b) 60 bins, (c) 120 bins, and (d) 240 bins.

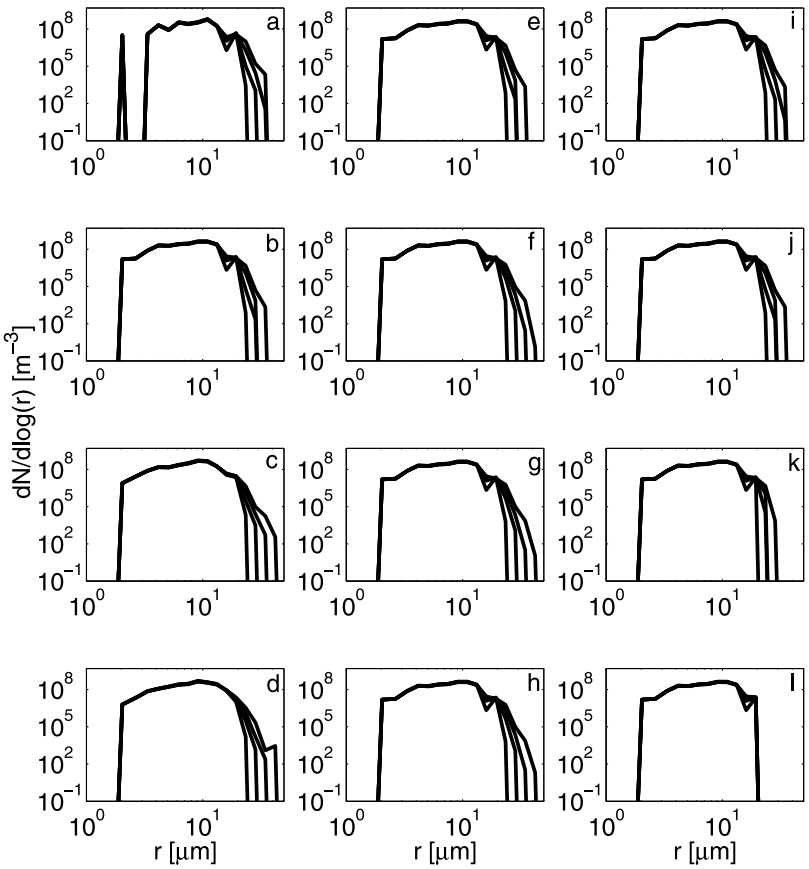

Figure 14. Sensitivity runs for the setup with 30 bins. Sensitivity to the number of parcels used to represent initial distribution: (a) 50, (b) 100, (c) 200, and (d) 500. Sensitivity to the number of parcels allowed in each bin in merging procedure: (e) 2, (f) 10, (g) 50, and (h) 100, for run with 100 parcels initially. Sensitivity to threshold level n^T: (i) $n^T = 1$, (j) $n^T = 12.5$, (k) $n^T = 10^4$, and (l) $n^T = 10^6$.

(parcel model runs) with each realization having a different initial cloud droplet distribution; Figure 11b shows the solution when only one realization with 100 parcels was used.

[41] Numerical solution shows a relatively good agreement with analytical solutions for the droplet number in each bin. Small underprediction of the growth of the biggest droplets is apparent at later times. Averaging over 100 runs was necessary to properly sample the initial distribution. Run with 100 parcels initially (Figure 11b) shows bigger differences in the initial condition and its subsequent evolution. The differences at later times come from the undersampling of the initial droplet distribution. To investigate the impact of the sampling error, simulations with different number of parcels were conducted. Figure 12 shows the RMS error of the number of droplets normalized by the total number of droplets as a function of the nondimensional time $\tau = 1 - \exp^{-bN0v0t}$, with $b = 1.53 \times 10^3$ s^{-1} and $N_0v_0 = 1$. The error for simulations with 50, 100 and 200 parcels used to sample the initial distribution are shown, together with the error for solution averaged over 100 realizations each applying 100 parcels. Results indicate that, for early times, the error in the solution is determined by the sampling error (i.e., resulting from the representation of continuous function by discrete parcels). At later times, the error is increasing as a result of creation of new parcels (new ones are created only when a new parcel has at least 12.5 cloud droplets) and due to merging procedure.

[42] Figure 13 shows a comparison of the numerical solutions using the approach presented in this paper (without taking into account aerosol; i.e., using only 1D grid in the calculation of droplet collisions) with *Bott*'s [1998] approach applying the hydrodynamic kernel with *Long*'s [1974] collision efficiency, *Simmel et al.*'s [2002] drop terminal velocity formulation, and the bin structure defined by equation (1). An initial condition is the same as for the Golovin kernel simulation with 100 parcels. Figure 13 shows solutions after 200, 800, 1400 and 2000 s for simulations with dt = 0.1 s for various number of bins, from 30 to 240. The largest differences between the two methods are for 30 bins, with the parcel based scheme biggest radius after 2000 s around 35 μm and Bott's scheme already approaching 500 μm for the smallest concentration shown in Figure 13. With the increasing number of bins, however, both solutions tend to converge to the same solution, with the parcel based scheme extending to larger and larger sizes, and Bott's scheme limiting the extent of the distribution in the large size range. This is because Bott's scheme is diffusive by design (it transfers water to the neighboring bin during calculations) while the proposed scheme underpredicts collisional growth due to the way new parcels are created/merged and because of the sampling issues. The latter is highlighted by

the oscillations in the tail of the parcel-based solutions as a result of the discrete representation of the continuous function with the finite number of parcels.

[43] The parcel-based solution depends not only on the number of bins used to map collisions, but also on the number of parcels used to represent initial cloud droplet distribution, the threshold level defining smallest number of droplets each parcel represents, and the number of parcels allowed in each bin when parcel merging is completed. The sensitivity of the model solution to these three parameters is presented in Figure 14 for simulations with 100 parcels, 30 radius bins used to map collisions, and the setup as used in Figure 13a. The model solution shows smaller sensitivity to changes in these parameters than for changes in the number of bins. The scheme produces the largest drop sizes for the simulation with the largest number of parcels used to represent initial distribution, the largest number of parcels allowed in each bin, and the smallest threshold level.

[44] Overall, the tests presented here provide justification for the numerical implementation of the scheme as used in the LES simulations discussed in the paper, where not only accuracy of the scheme, but also overall model efficiency must be taken into account.

[45] **Acknowledgments.** This work was supported by NERC funding for the VOCALS project, NCAS computer time on HECToR, and BADC data centre. W.W.G. acknowledges support from NOAA grant NA08OAR4310543 and DOE ARM grant DE-FG02-08ER64574.

References

Ackerman, A. S., P. V. Hobbs, and O. B. Toon (1995), A model for particle microphysics, turbulent mixing, and radiative transfer in the stratocumulus-topped marine boundary layer and comparisons with measurements, *J. Atmos. Sci.*, *52*, 1204–1236.

Ackerman, A. S., M. P. Kirkpatrick, D. E. Stevens, and O. B. Toon (2004), The impact of humidity above stratiform clouds on indirect aerosol climate forcing, *Nature*, *342*, 1014–1017.

Ackerman, A. S., et al. (2009), Large-eddy simulations of a drizzling, stratocumulus-topped marine boundary layer, *Mon. Weather Rev.*, *137*, 1083–1110.

Andrejczuk, M., W. W. Grabowski, S. P. Malinowski, and P. K. Smolarkiewicz (2004), Numerical simulation of cloud-clear air interfacial mixing, *J. Atmos. Sci.*, *61*, 1726–1739.

Andrejczuk, M., W. W. Grabowski, S. P. Malinowski, and P. K. Smolarkiewicz (2006), Numerical simulation of cloud-clear air interfacial mixing: Effects on cloud microphysics, *J. Atmos. Sci.*, *63*, 3204–3225.

Andrejczuk, M., J. M. Reisner, B. F. Henson, M. Dubey, and C. A. Jeffery (2008), The potential impacts of pollution on a nondrizzling stratus deck: Does aerosol number matter more than type?, *J. Geophys. Res.*, *113*, D19204, doi:10.1029/2007JD009445.

Andrejczuk, M., W. W. Grabowski, S. P. Malinowski, and P. K. Smolarkiewicz (2009), Numerical simulation of cloud-clear air interfacial mixing: Homogeneous versus inhomogeneous mixing, *J. Atmos. Sci.*, *66*, 2493–2500.

Bott, A. (1998), A flux method for the numerical solution of the stochastic collection equation, *J. Atmos. Sci.*, *55*, 2284–2293.

Bott, A. (2000), A flux method for the numerical solution of the stochastic collection equation: Extension to two-dimensional particle distributions, *J. Atmos. Sci.*, *57*, 284–294.

Brenguier, J.-L., and W. W. Grabowski (1993), Cumulus entrainment and cloud droplet spectra: A numerical model within a two-dimensional dynamical framework, *J. Atmos. Sci.*, *50*, 120–136.

Bretherton, C. S., P. N. Blossey, and J. Uchida (2007), Cloud droplet sedimentation, entrainment efficiency, and subtropical stratocumulus albedo, *Geophys. Res. Lett.*, *34*, L03813, doi:10.1029/2006GL027648.

Chen, J.-P., and D. Lamb (1994), Simulation of cloud microphysical and chemical processes using a multicomponent framework. Part I: Description of the microphysical model, *J. Atmos. Sci.*, *51*, 2613–2630.

Clark, T. L. (1973), Numerical modeling of the dynamics and microphysics of warm cumulus convection, *J. Atmos. Sci.*, *30*, 857–878.

Golovin, A. M. (1963), The solution of the coagulation equation for cloud dropletsin a rising air current, *Bull. Acad. Sci. USSR, Geophys. Ser. (Engl. Transl.)*, *5*, 482–487.

Hill, A. A., G. Feingold, and H. Jiang (2009), The influence of entrainment and mixing assumption on aerosol-cloud interactions in marine stratocumulus, *J. Atmos. Sci.*, *66*, 1450–1464.

Intergovernmental Panel on Climate Change (2007), *Climate Change 2007: Synthesis Report*, report, 104 pp., Geneva.

Jacobson, M. Z., R. P. Turco, E. J. Jensen, and O. B. Toon (1994), Modeling coagulation among particles of different composition and size, *Atmos. Environ., Part A*, *28*, 1327–1338.

Khain, A. P., A. Pokrovsky, M. Pinsky, A. Seifert, and V. Phillips (2004), Simulation of effects of atmospheric aerosols on deep turbulent convective clouds using a spectral microphysics mixed-phase cumulus cloud model. Part I: Model description and possible applications, *J. Atmos. Sci.*, *61*, 2963–2982.

Khairoutdinov, M. F., and Y. L. Kogan (1999), A large eddy simulation model with explicit microphysics: Validation against aircraft observations of a stratocumulus-topped boundary layer, *J. Atmos. Sci.*, *56*, 2115–2131.

Kogan, Y. L., M. F. Khairoutdinov, D. Lilly, Z. Kogan, and Q. Liu (1995), Modeling of stratocumulus cloud layers in a large eddy simulation model with explicit microphysics, *J. Atmos. Sci.*, *52*, 2923–2940.

Leroy, D., W. Wobrock, and A. I. Flossmann (2009), The role of boundary layer aerosol particles for the development of deep convective clouds: A high-resolution 3D model with detailed (bin) microphysics applied to CRYSTAL-FACE, *Atmos. Res.*, *91*, 62–78.

Long, A. B. (1974), Solutions to the droplet collection equation for polynomial Kernels, *J. Atmos. Sci.*, *31*, 1040–1052.

Morrison, H., and W. W. Grabowski (2007), Comparison of bulk and bin warm-rain microphysics models using a kinematic framework, *J. Atmos. Sci.*, *137*, 2839–2861.

Reisner, J. M., and C. A. Jeffery (2009), A smooth cloud model, *Mon. Weather Rev.*, *137*, 1825–1843.

Scott, W. D. (1963), Analytic studies of cloud droplet coalescence, *J. Atmos. Sci.*, *25*, 54–65.

Shima, S., K. Kusano, A. Kawano, T. Sugiyama, and S. Kawahara (2009), The super-droplet method for the numerical simulation of clouds and precipitation: A particle-based and probabilistic microphysics model coupled with a non-hydrostatic model, *Q. J. R. Meteorol. Soc.*, *135*, 1307–1320.

Simmel, M., T. Trautmann, and G. Tetzlaff (2002), Numerical solution of the stochastic collection equation comparison of the linear discrete method with other methods, *Atmos. Res.*, *61*, 135–148.

Stevens, B., W. R. Cotton, G. Feingold, and C.-H. Moeng (1998), Large-eddy simulations of strongly precipitating, shallow, stratocumulus-topped boundary layers, *J. Atmos. Sci.*, *55*, 3616–3638.

Stevens, B., et al. (2003), On entrainment rates in nocturnal marine stratocumulus, *Q. J. R. Meteorol. Soc.*, *129*, 3469–3493.

Stevens, B., et al. (2005), Evaluation of large-eddy simulations via observations of nocturnal marine stratocumulus, *Mon. Weather Rev.*, *133*, 1443–1462.

Turton, J. D., and S. Nicholls (1987), A study of the diurnal variation of stratocumulus using a multiple mixed layer model, *Q. J. R. Meteorol. Soc.*, *113*, 969–1009.

Twohy, C. H., M. D. Petters, J. R. Snider, B. Stevens, W. Tahnk, M. Wetzel, L. Russell, and F. Burnet (2005), Evaluation of the aerosol indirect effect in marine stratocumulus clouds: Droplet number, size, liquid water path, and radiative impact, *J. Geophys. Res.*, *110*, D08203, doi:10.1029/2004JD005116.

Wang, L.-P., and W. W. Grabowski (2009), The role of air turbulence in warm rain Initiation, *Atmos. Sci. Lett.*, *10*, 1–8.

M. Andrejczuk and A. Gadian, School of Earth and Environment, University of Leeds, Leeds LS2 9JT, UK. (m.andrejczuk@leeds.ac.uk)

W. W. Grabowski, Mesoscale and Microscale Meteorology Division, National Center for Atmospheric Research, Boulder, CO 80305, USA.

J. Reisner, Earth and Environmental Sciences Division, Los Alamos National Laboratory, Los Alamos, NM 87544, USA.